

Módulo 2

Sistemas monzónicos

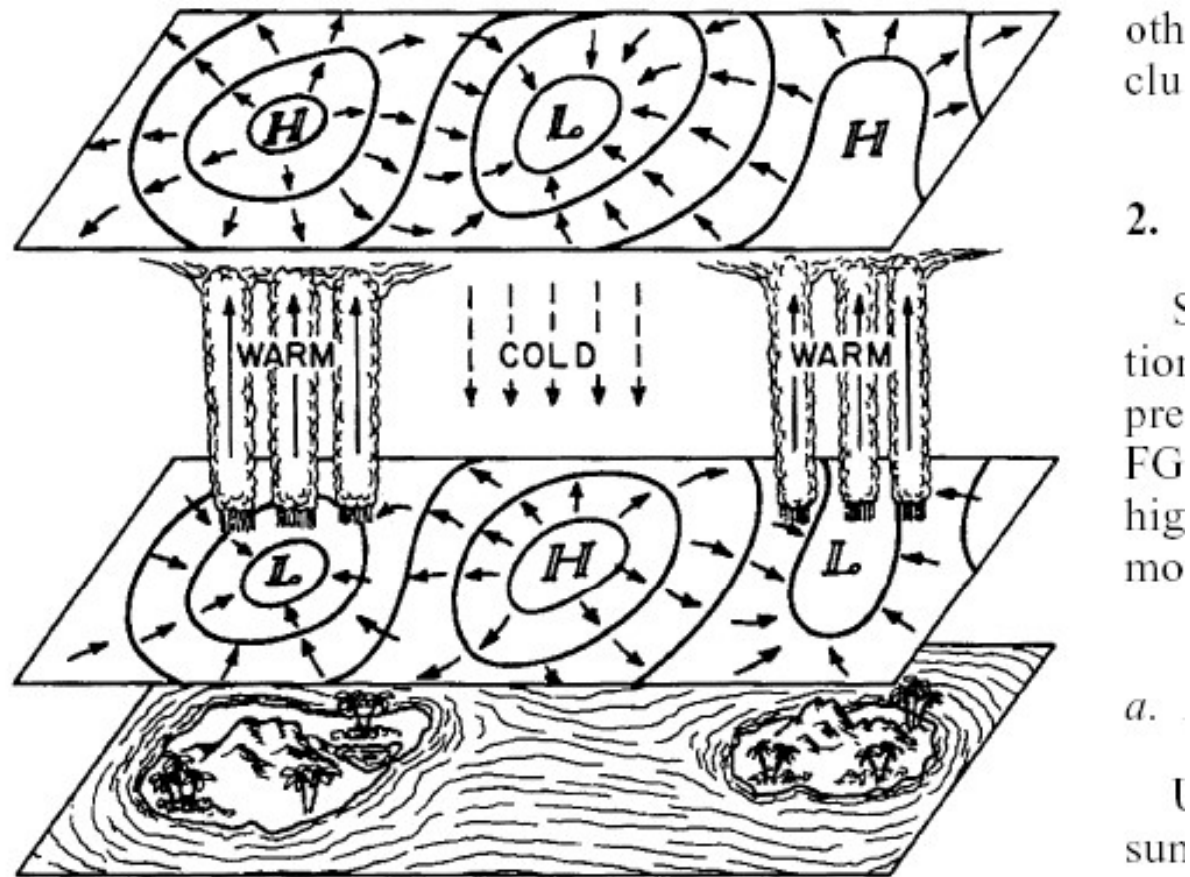


FIG. 1. An idealized summer monsoon circulation depicted by Wallace and Hobbs (1977). Tropical continents are represented by islands, while the high (H) and low (L) systems near sea level (lower plane) and 200 mb (upper plane) are portrayed by geopotential contours. Cross-isobar divergent (convergent) flows (short arrows) and vertical motions in the midtroposphere (vertical arrows).

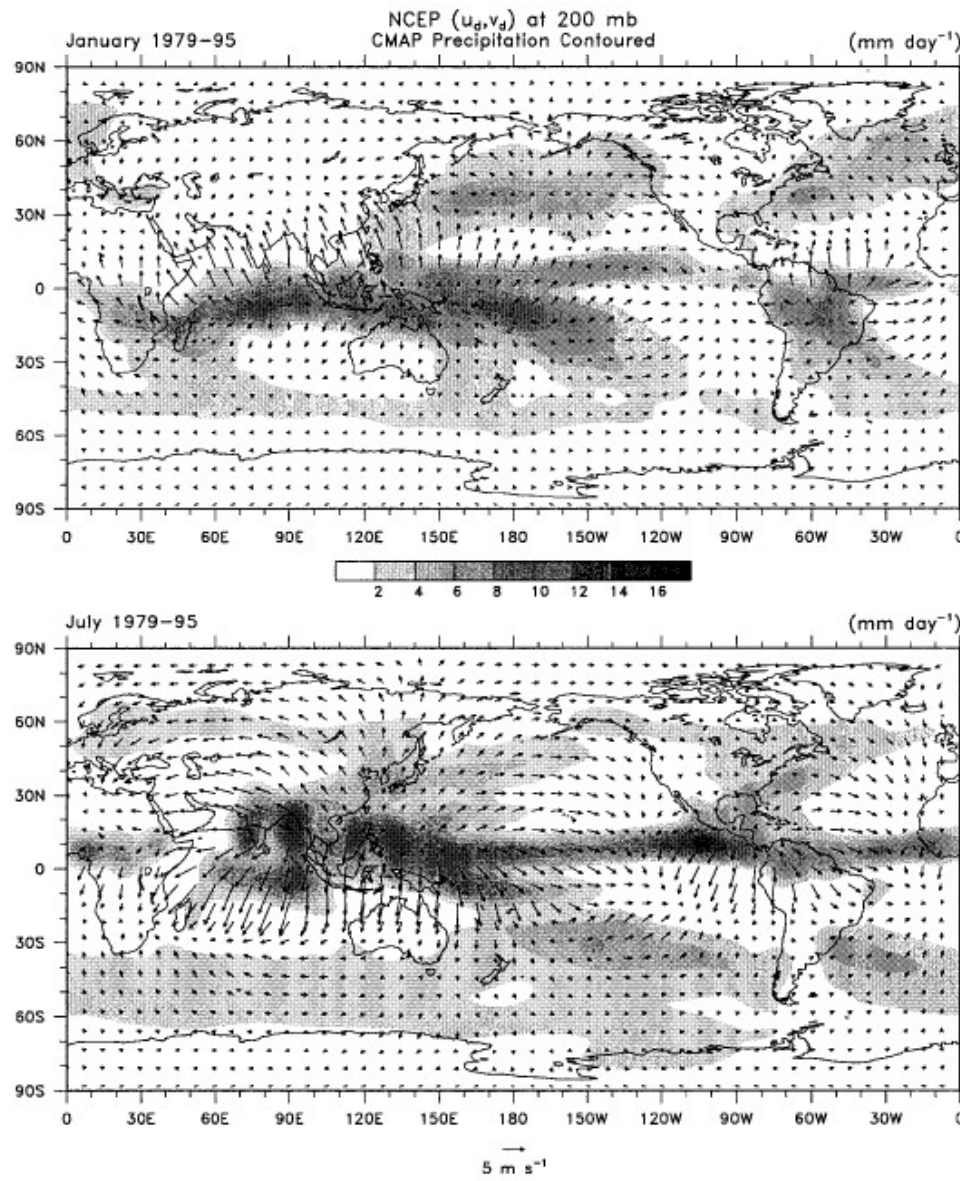


FIG. 8. For 1979–95, mean precipitation in mm day^{-1} from the CMAP analysis along with the NCEP 200-mb divergent wind component in m s^{-1} , with the scale vector below each plot for Jan and Jul. The grayscale increments in 2 mm day^{-1} and values less than 2 mm day^{-1} are left blank.

Monsoon Systems

Seasonal phenomenon responsible for producing the majority of wet season rainfall within the tropics. The precipitation characteristics over the Asian-Australian, American and African monsoons can be viewed as an integrated global monsoon system, associated with a global-scale atmospheric overturning circulation.

Trenberth et al., 2000

CIRCULACION DIVERGENTE Y CALENTAMIENTO DIABATICO

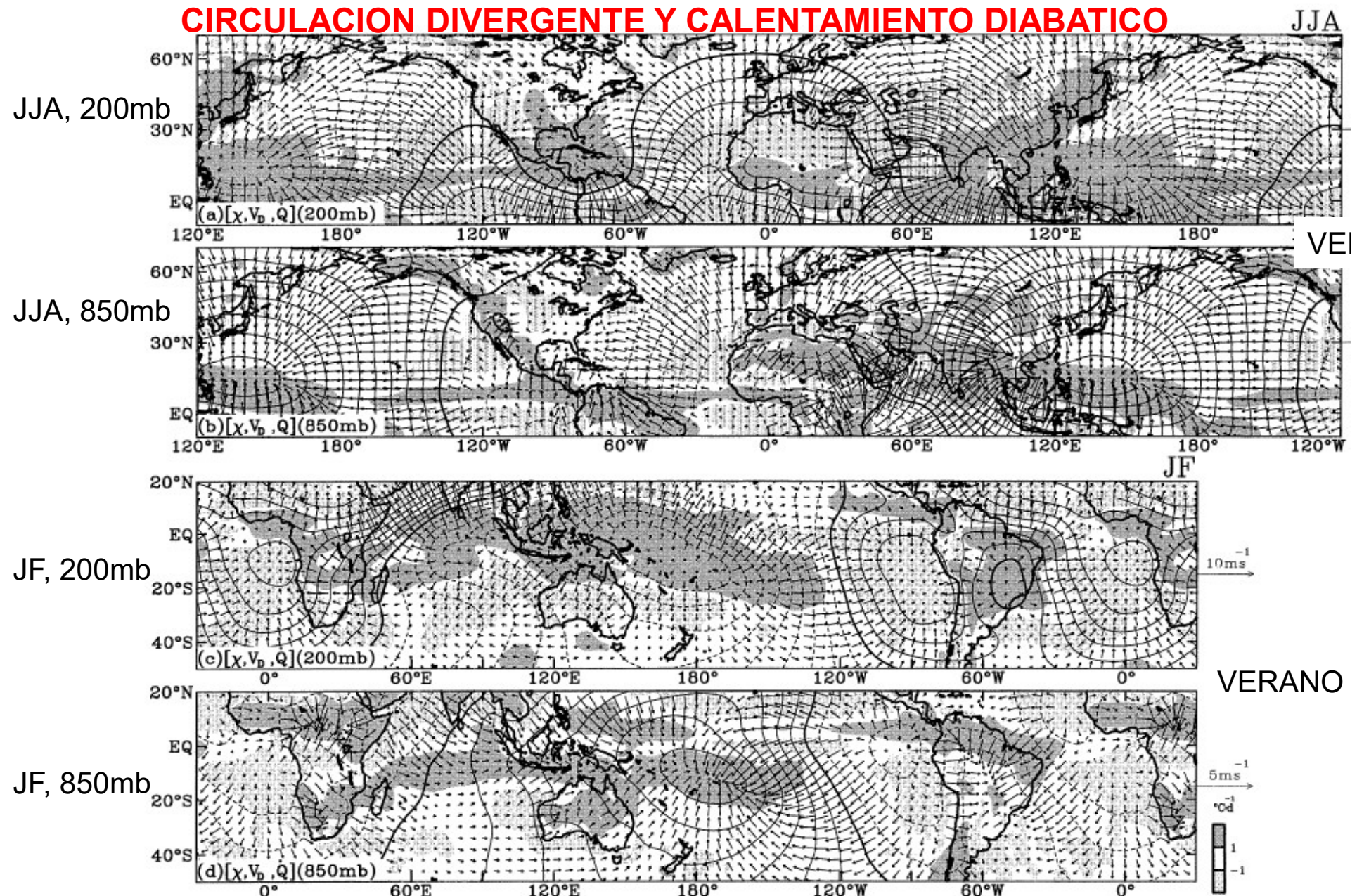
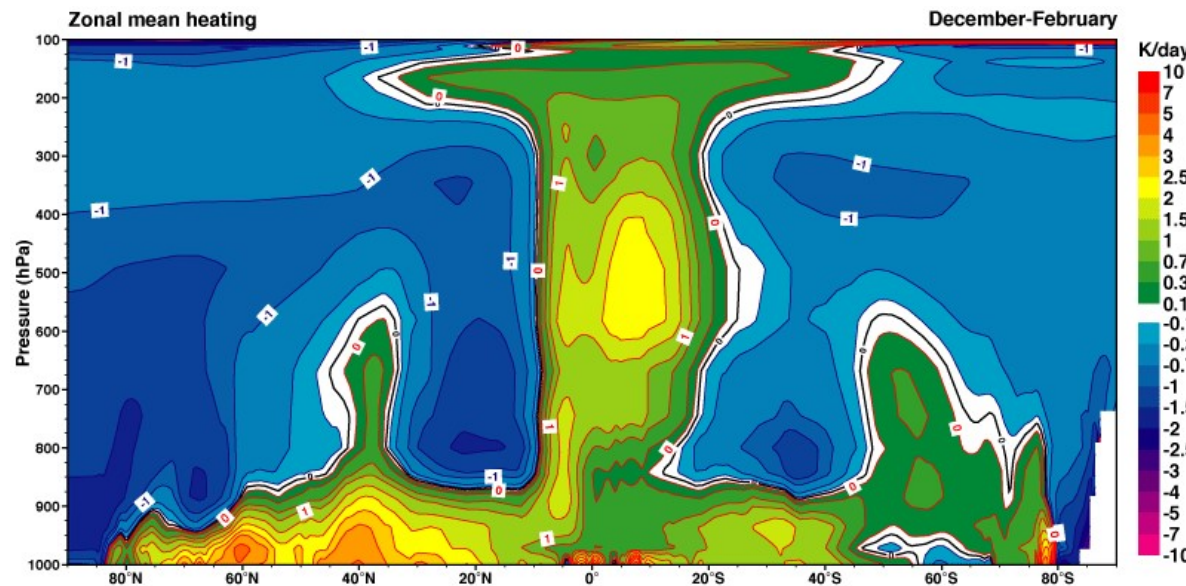


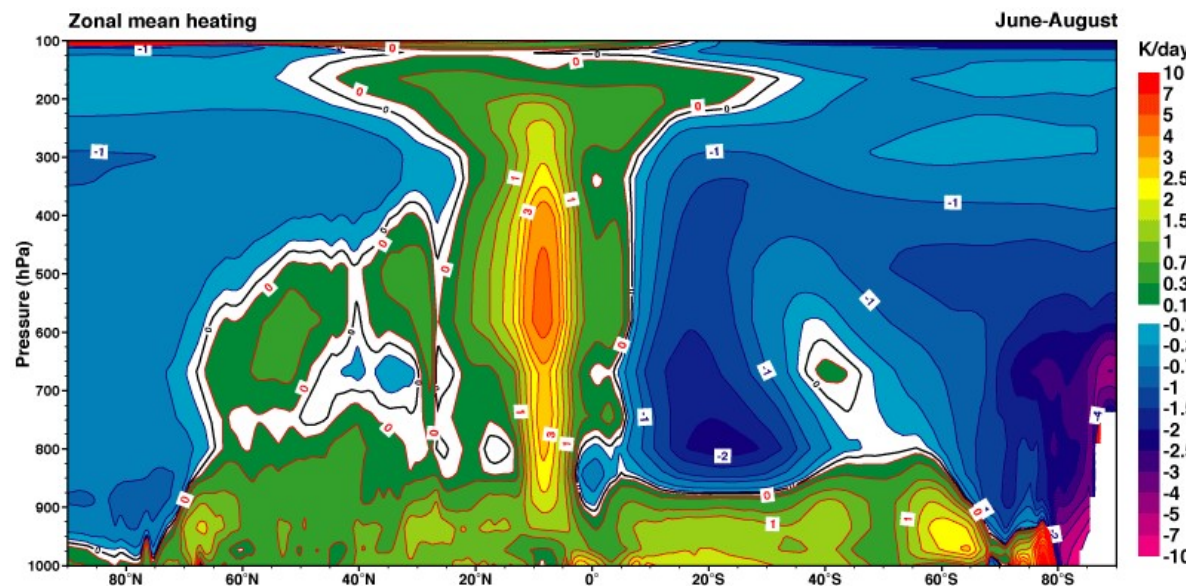
FIG. 3. Divergent circulation (χ , V_D) superimposed with diabatic heating (\dot{Q}) during the northern summer (JJA) at (a) 200 mb 850 mb, and during the winter (JF) at (c) 200 mb and (d) 850 mb. Positive (negative) values of \dot{Q} larger (smaller) than 1°C day^{-1} Chen, 2003, Maintenance of Summer Monsoon Circulations: A Planetary-Scale Perspective, J.Climate 1 (b)-(d).

Distribución global de calentamiento y enfriamiento diabático (media zonal)

DJF

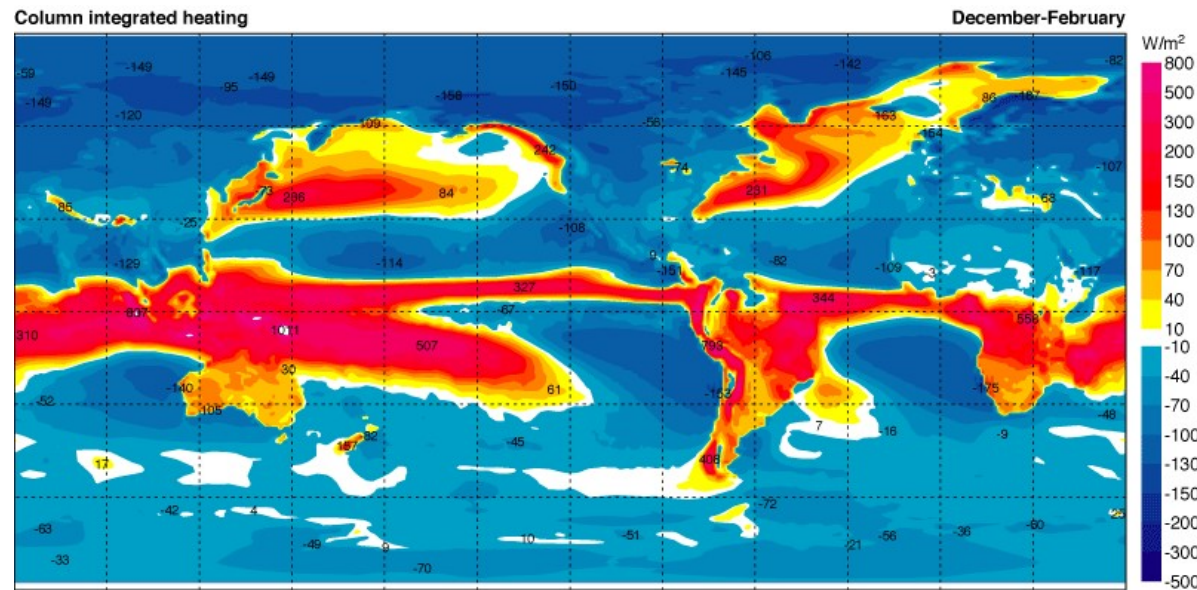


JJA

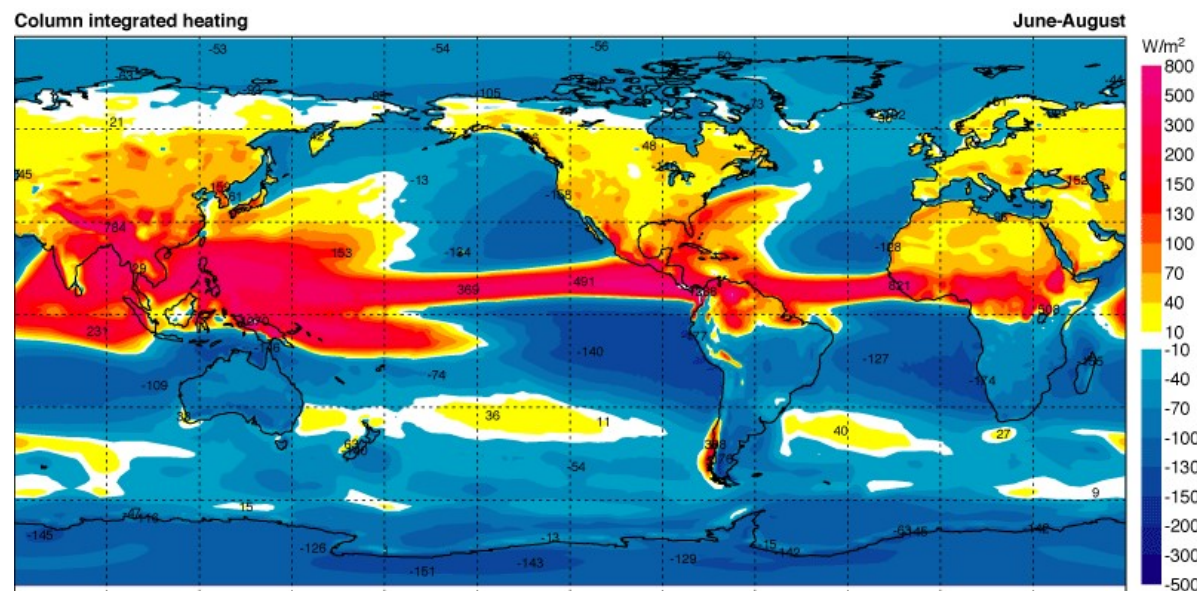


Distribución global de calentamiento y enfriamiento diabático (integrado verticalmente)

DJF



JJA



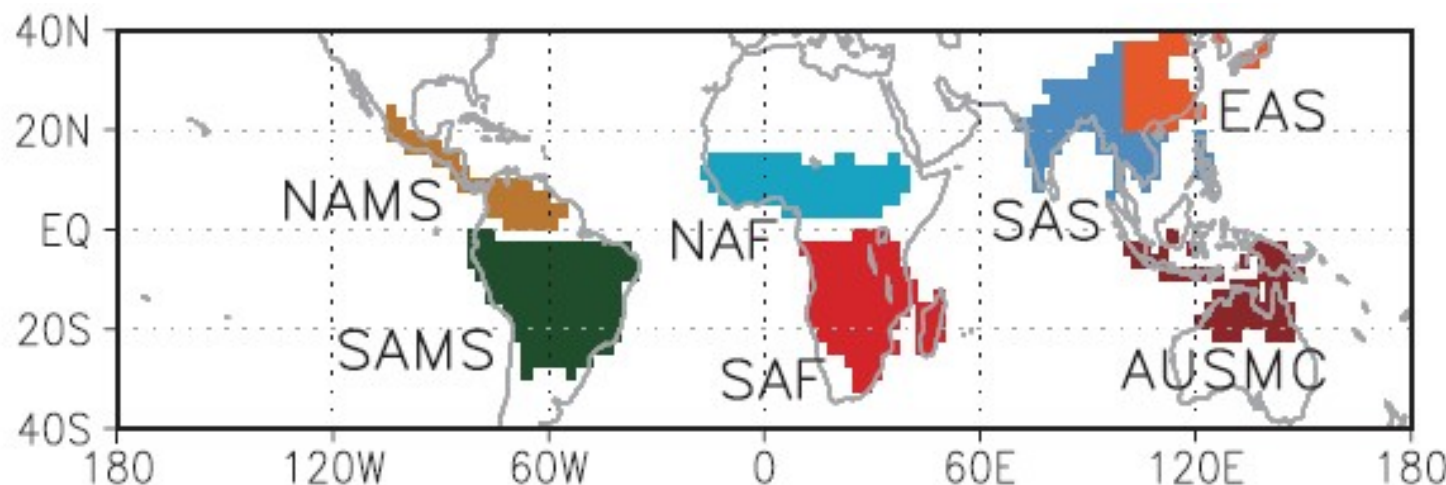


Figure 14.3 | Regional land monsoon domain based on 26 CMIP5 multi-model mean precipitation with a common $2.5^\circ \times 2.5^\circ$ grid in the present-day (1986–2005). For regional divisions, the equator separates the northern monsoon domains (North America Monsoon System (NAMS), North Africa (NAF), Southern Asia (SAS) and East Asian summer (EAS)) from the southern monsoon domains (South America Monsoon System (SAMS), South Africa (SAF), and Australian-Maritime Continent (AUSMC)), 60°E separates NAF from SAS, and 20°N and 100°E separates SAS from EAS. All the regional domains are within 40°S to 40°N.

Dynamical Theory

P J Webster and J Fasullo, University of Colorado –
Boulder, Boulder, CO, USA

Copyright 2003 Elsevier Science Ltd. All Rights Reserved.

Los monzones surgen del desarrollo de **gradientes de presión cros-ecuatoriales** producidos o modificados por los siguientes procesos y propiedades físicas del **sistema tierra-océano-atmósfera**:

- 1) El **calentamiento diferencial** de la tierra y el océano producido por la diferente capacidad de calor de la tierra y el agua;
- 2) Las diferencias en **la transferencia vertical de calor y en su almacenamiento** en el océano y la tierra;
- 3) La modificación del calentamiento diferencial por **procesos húmedos**;
- 4) La generación de **fuerzas de gradiente de presión** meridional resultantes del calentamiento diferencial; y
- 5) El **transporte meridional de calor en el océano** por procesos dinámicos.

Cada uno de estos procesos y propiedades tiene que ser considerado en relación con la **rotación del planeta**, y la influencia de efectos locales como la geografía del océano y las masas de tierra, y la topografía regional.

Generación de fuerzas de gradiente de presión monzónicas

Combinando la ecuación de estado y la ecuación hidrostática:

$$\frac{\partial p}{\partial z} = -\frac{g}{R} \frac{p}{\bar{T}} \quad [4]$$

donde \bar{T} es la temperatura media de una columna atmosférica. Integrando para una columna sobre continente (w: warm) y otra sobre océano (c: cold), y restando:

$$\Delta \ln p(z_1) = \frac{g}{R} z_1 \left(\frac{1}{\bar{T}_c} - \frac{1}{\bar{T}_w} \right) + \Delta \ln p(0) \quad [5]$$

En superficie: $p(w) < p(c) \rightarrow \Delta \ln p(0) < 0$ (el delta es warm – cold)

Para que exista revertimiento de la circulación con la altura: $\Delta \ln p(z_1) > 0$,

Es decir, la columna de atmósfera sobre continente debe tener una temperatura media que supere el siguiente umbral :

$$\bar{T}_w > \frac{gz_1 \bar{T}_c}{gz_1 + R \Delta \ln p(0) \bar{T}_c} \quad [6]$$

$T(w)$ supera este umbral solo cuando tenemos liberación de calor latente por la convección

Intensificación del gradiente de presión cros-ecuatorial

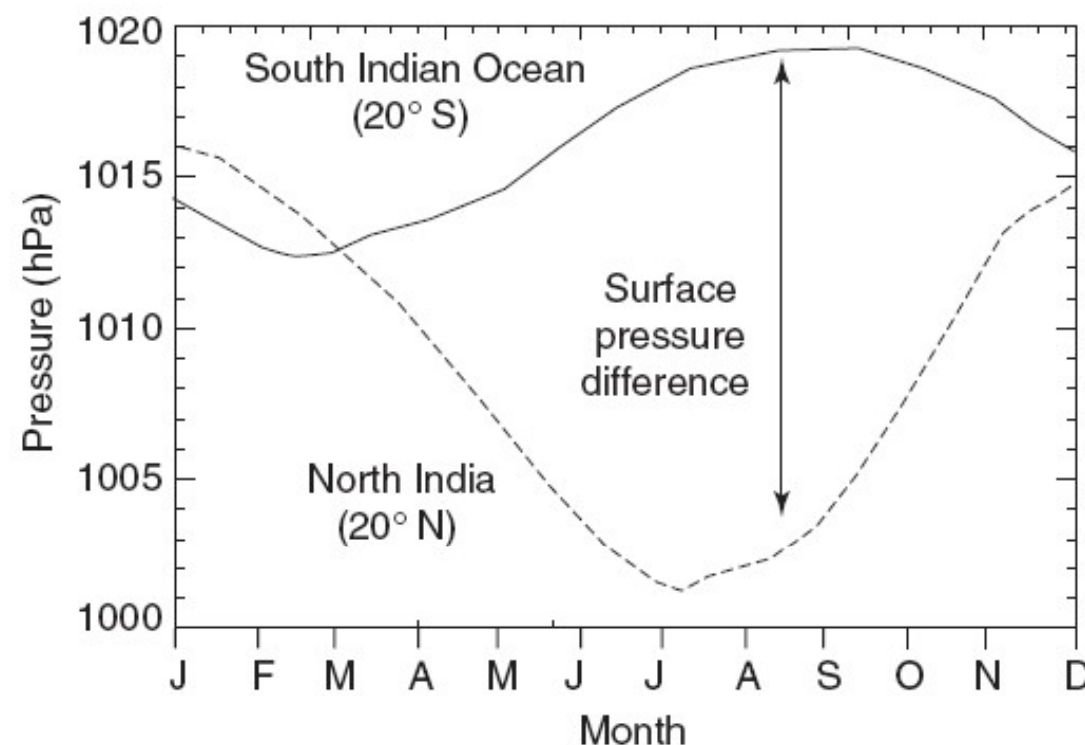


Figure 3 The mean annual cycle of sea-level pressure at 20° N and 20° S along 80° E, representing the monsoon trough and South Indian Ocean, respectively.

Flujo de humedad integrado verticalmente

$$I = \int_0^{\infty} q \tilde{V} dz$$

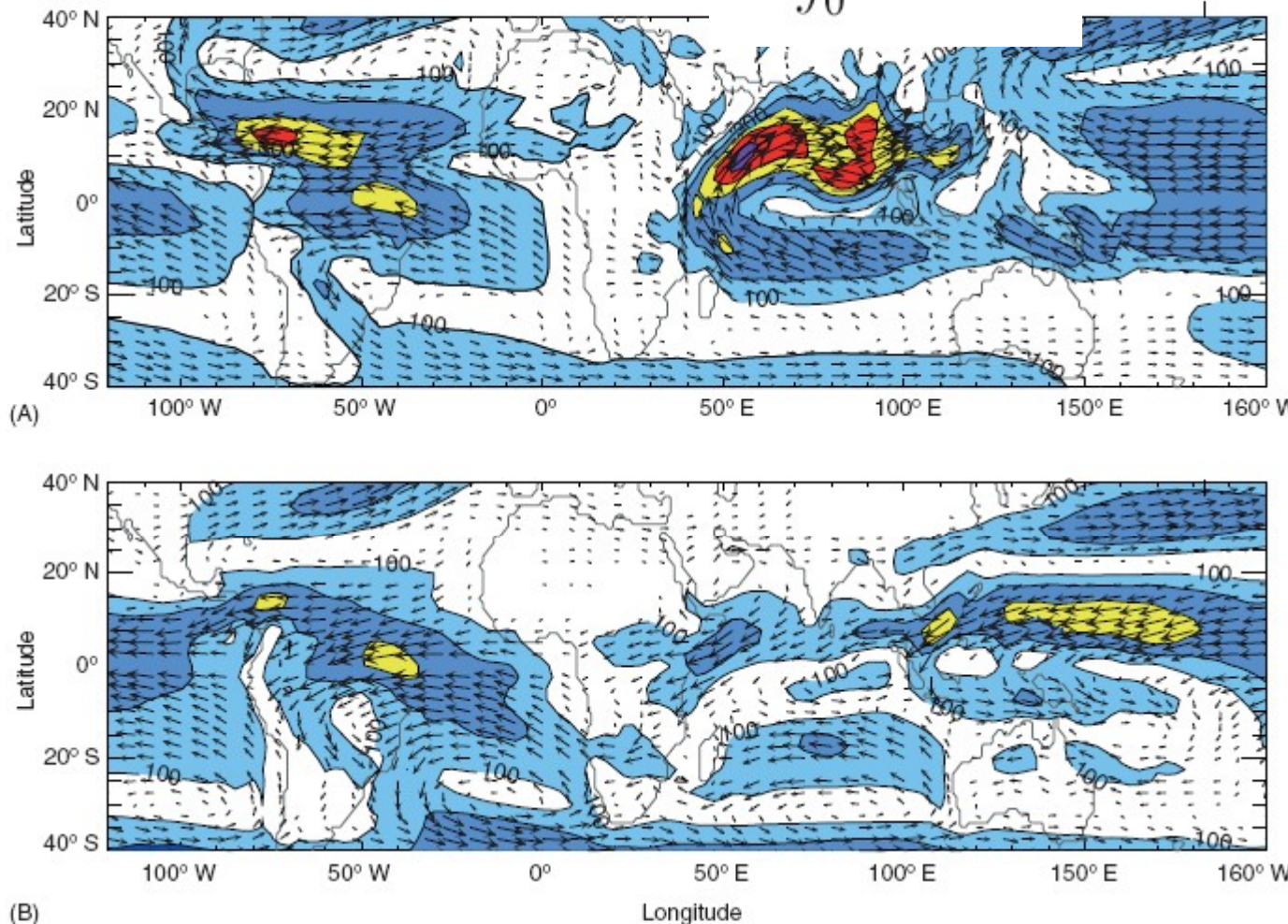
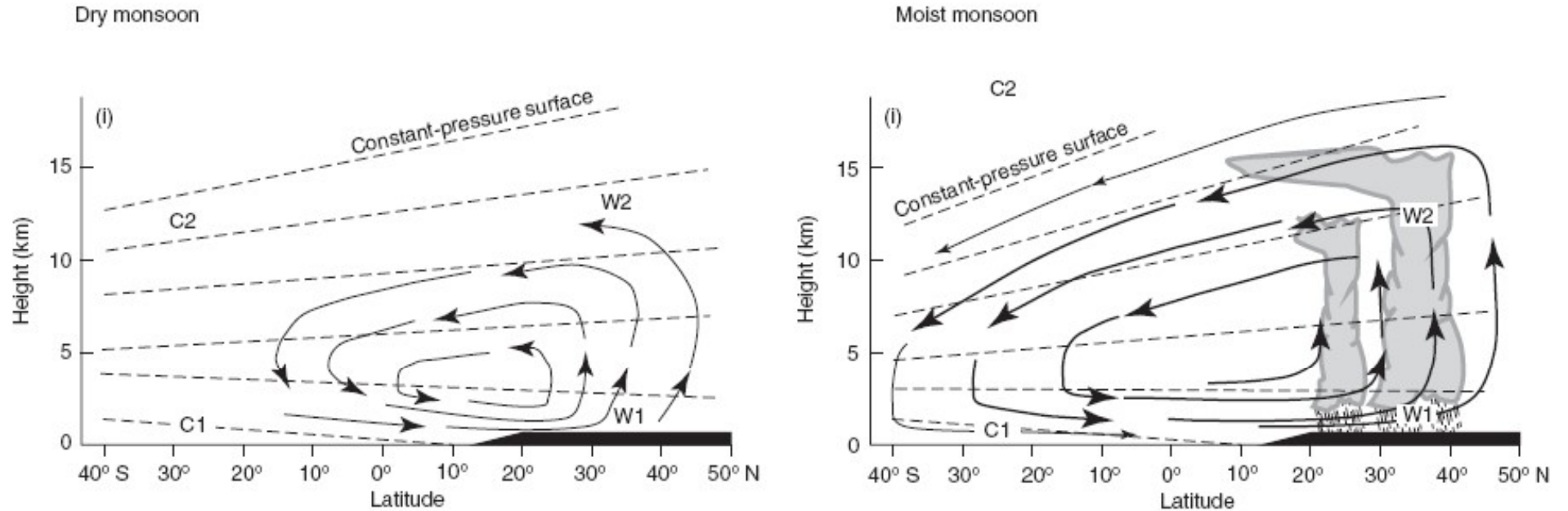


Figure 4 Distribution of mean vertically integrated moisture transport from eqn [7] for the period (A) June–September and (B) December–February. Viewed in the context of moisture transport, the Asian–Australian monsoon system appears in both (A) the boreal summer and (B) the boreal winter as strong interhemispheric systems with moisture sources clearly defined in the winter hemisphere. Both the African summer and winter monsoons are less clearly defined. Weak moisture fluxes into north-west Africa are evident, for example, but the region is dominated by strong westward moisture fluxes associated with the Trade Wind across the Atlantic. Furthermore, the moisture fluxes associated with the North and South American monsoons appear restricted to their respective hemispheres. Only the Asian–Australian monsoon possesses a truly interhemispheric solar collector.

Webster & Fasullo, 2003: Monsoon/Dynamical Theory



Desarrollo de la circulación meridional monzónica: (A) cuando se ignoran los procesos húmedos y (B) cuando se tienen en cuenta los procesos húmedos

Efecto de la fuerza de Coriolis

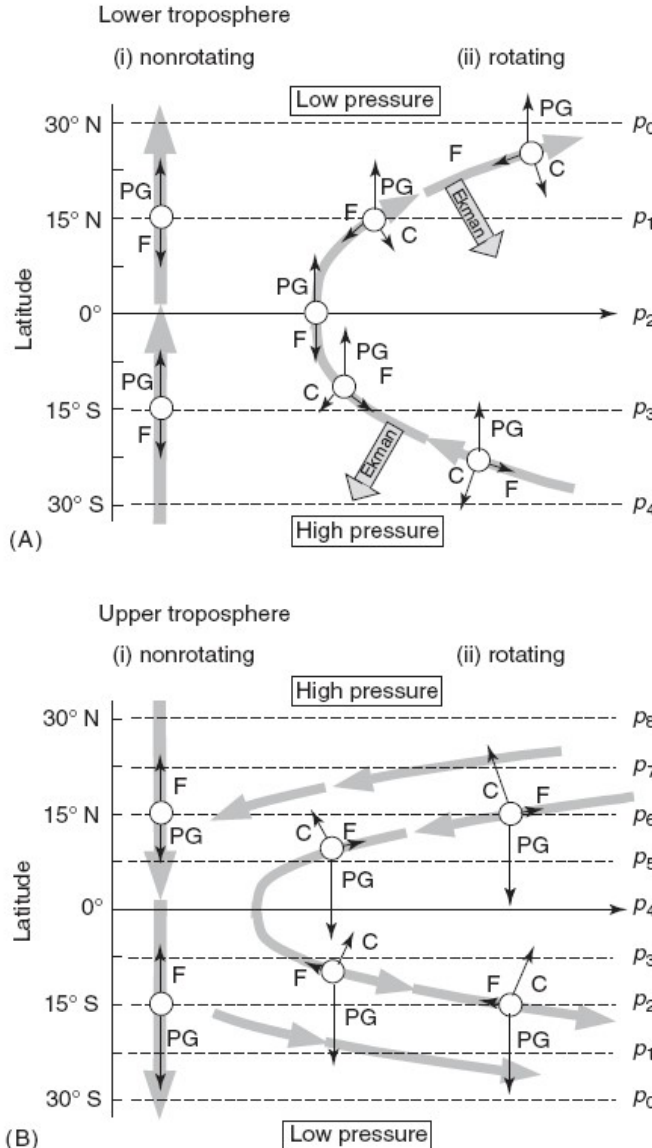


Figure 5 The circulation across the Equator in (A) the lower troposphere and (B) the upper troposphere on (i) a nonrotating planet, and (B) a rotating planet. Circulation is forced by a pressure-gradient force (PG) that is constant in latitude and subject to Coriolis effects (C) and frictional dissipation (F) that is assumed to be proportional to the parcel speed. The broad arrows denote the integrated Ekman mass ocean transport forced by the surface winds.

$$\frac{d\mathbf{V}}{dt} = -\frac{1}{\rho} \nabla p - f \mathbf{k} \times \mathbf{V} - \alpha \mathbf{V}$$

Webster & Fasullo, 2003:
Monsoon/Dynamical Theory

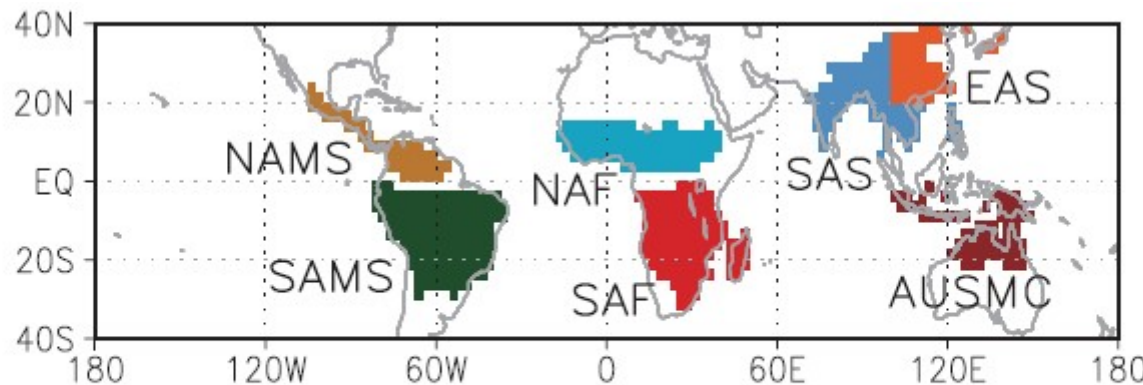
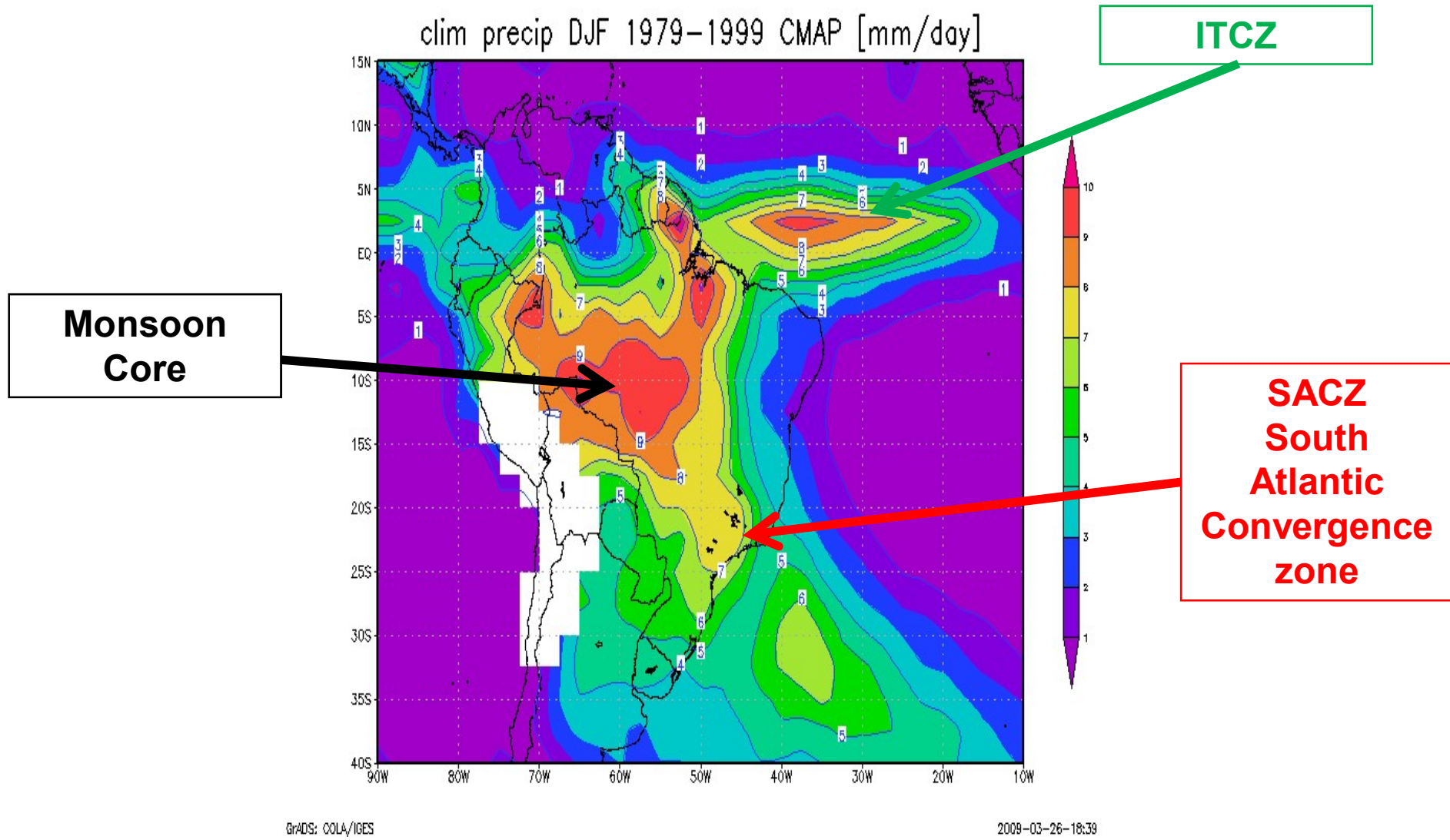


Figure 14.3 | Regional land monsoon domain based on 26 CMIP5 multi-model mean precipitation with a common $2.5^\circ \times 2.5^\circ$ grid in the present-day (1986–2005). For regional divisions, the equator separates the northern monsoon domains (North America Monsoon System (NAMS), North Africa (NAF), Southern Asia (SAS) and East Asian summer (EAS)) from the southern monsoon domains (South America Monsoon System (SAMS), South Africa (SAF), and Australian-Maritime Continent (AUSMC)), 60°E separates NAF from SAS, and 20°N and 100°E separates SAS from EAS. All the regional domains are within 40°S to 40°N .

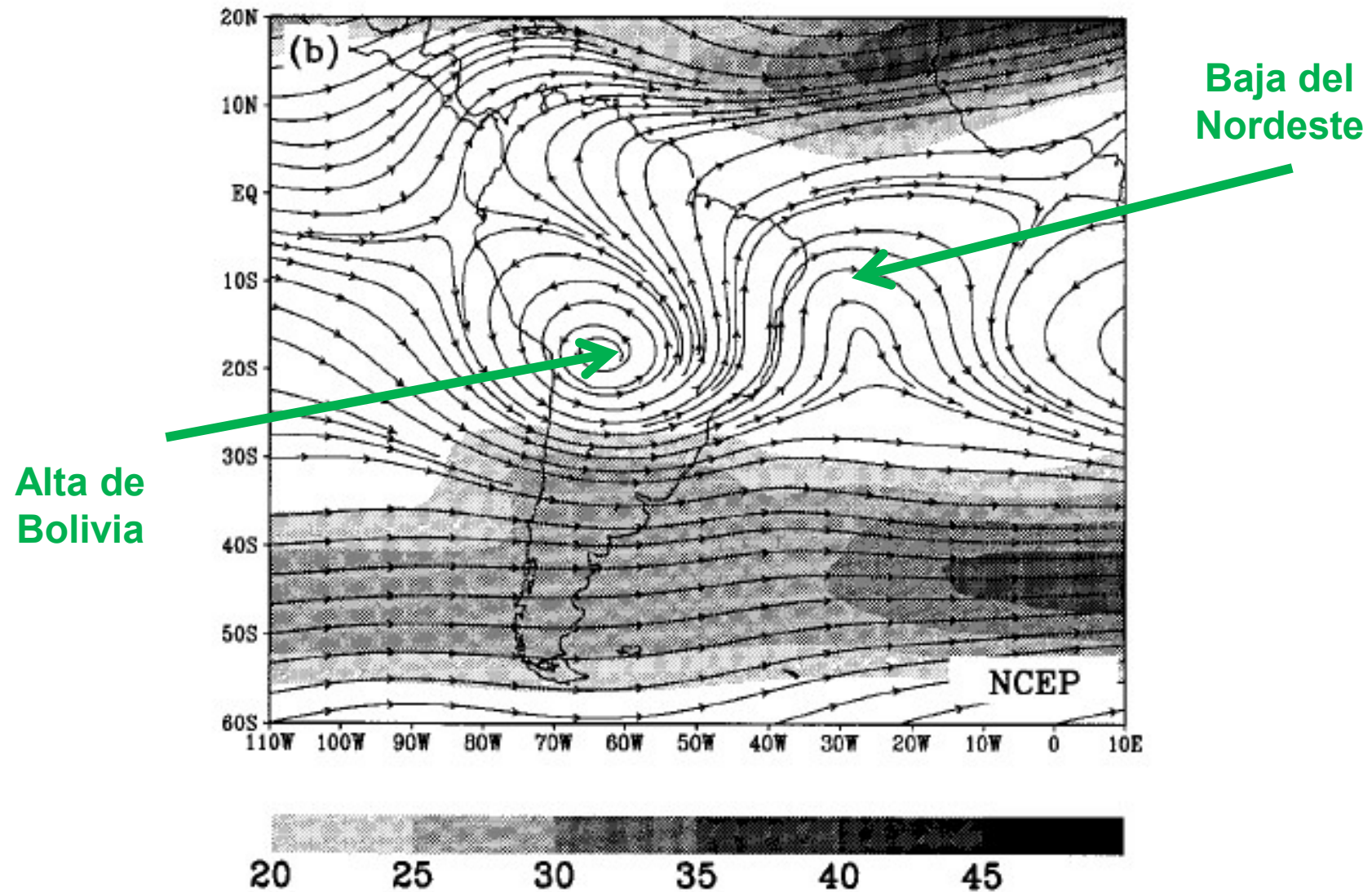
The main characteristics of SAMS onset are increased humidity flux from the Atlantic Ocean over northern South America, an eastward shift of the subtropical high, strong northwesterly moisture flux east of the tropical Andes, and establishment of the Bolivian High (Raia and Cavalcanti, 2008; Marengo et al., 2010a; Silva and Kousky, 2012).



DJF climatological mean precipitation

Circulación en 200 hPa de DJF

(Líneas de corriente&isotacas)



Zhou & Lau, 1998: Does a Monsoon Climate Exist over South America? (J.Clim.)

Principales
características de los
sistemas monzónicos de
Sudamérica y Asia

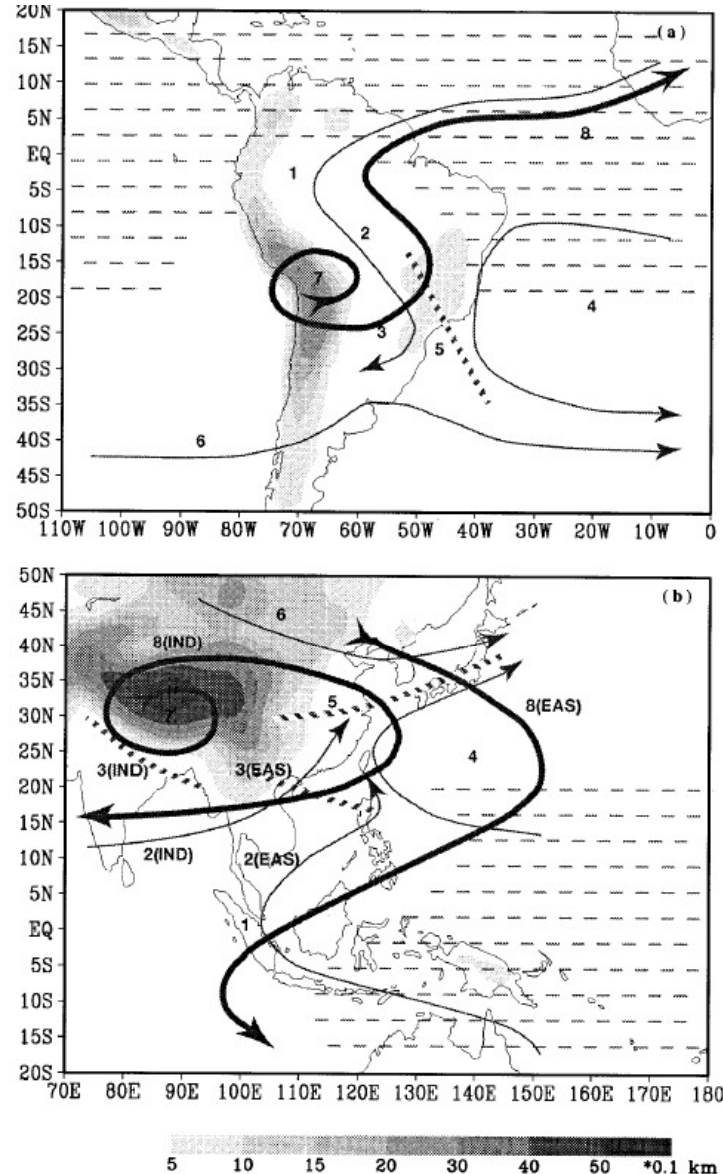


FIG. 18. Schematic illustration of elementary features for (a) SASM and (b) EASM. The shading represents the topography. The areas where easterlies prevail are indicated by dashed lines. The correspondingly numbered features are as follows: 1) low-level cross equatorial flow, 2) northeasterlies vs southwesterlies, 3) Gran Chaco low vs EASM trough, 4) subtropical high, 5) SACZ vs Mei-Yu front zone, 6) midlatitude westerlies, 7) Bolivian high vs Tibetan high, and 8) upper-level return flow.

PROCESOS QUE AFECTAN LA CONVECCION SOBRE SUDAMERICA EN VERANO

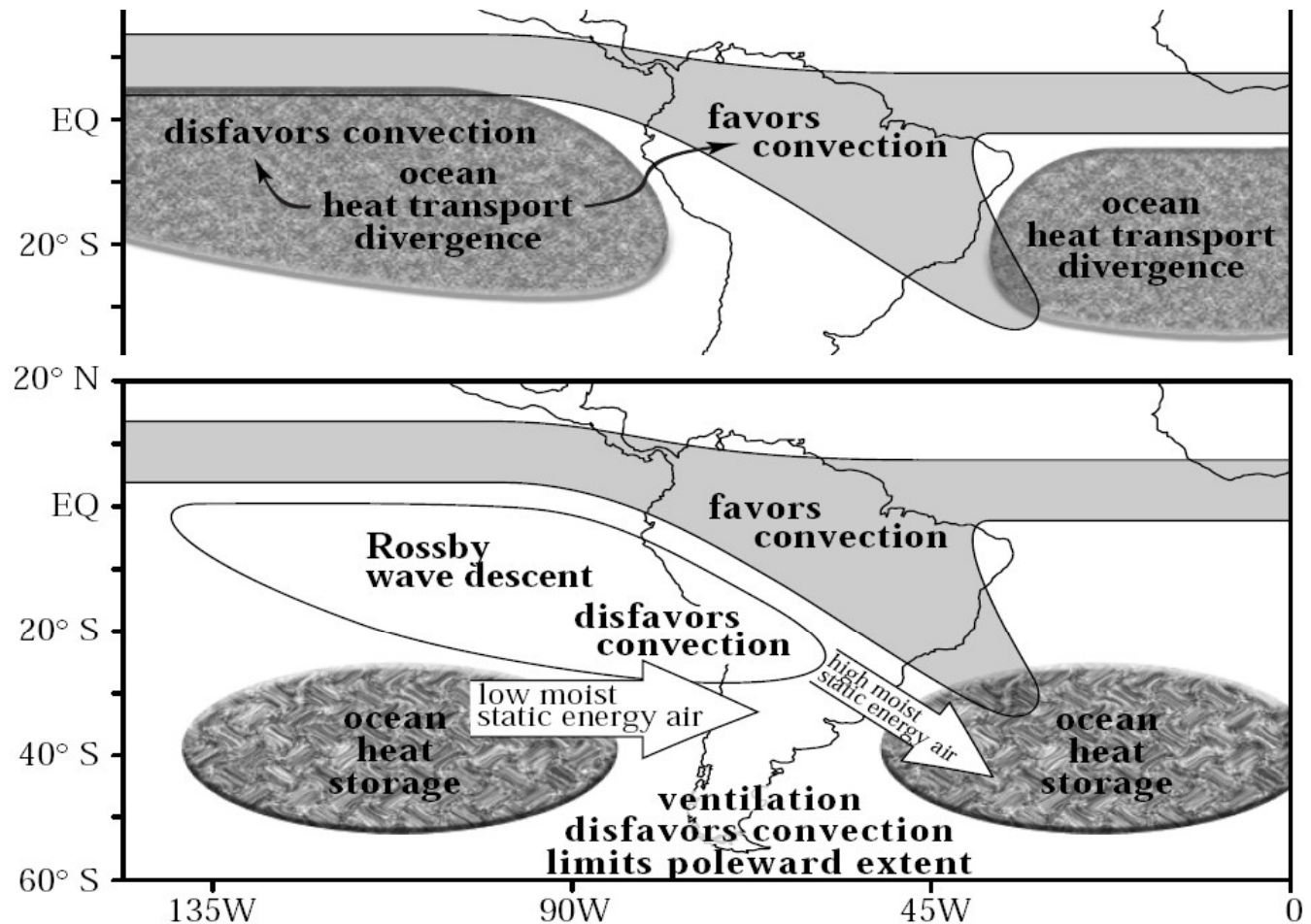
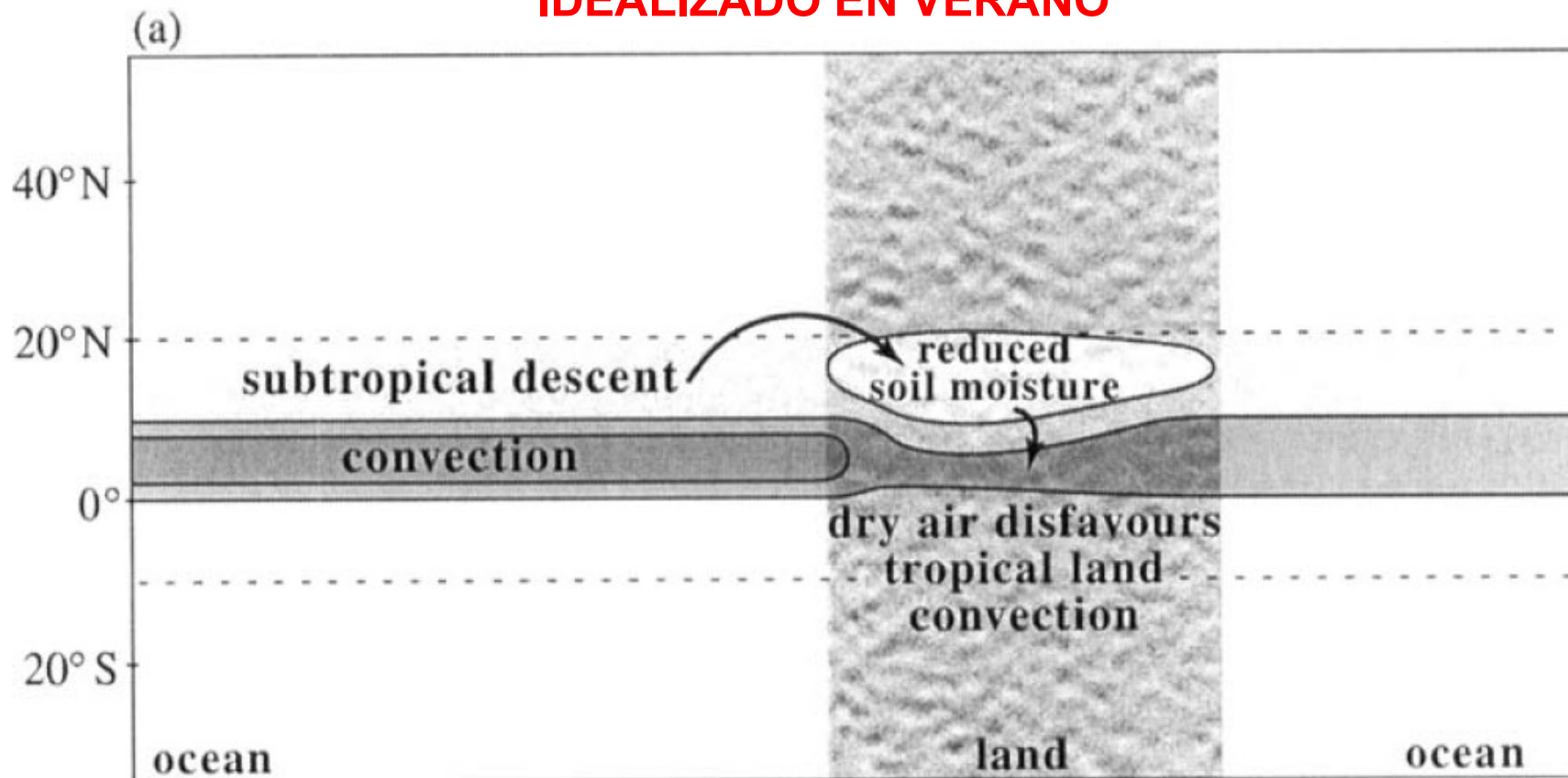


Fig. 11. Schematic of mechanisms relevant to large-scale aspects of the South American summer monsoon, following Chou and Neelin (2001), including the "interactive Rodwell-Hoskins" and the "ventilation" mechanisms.

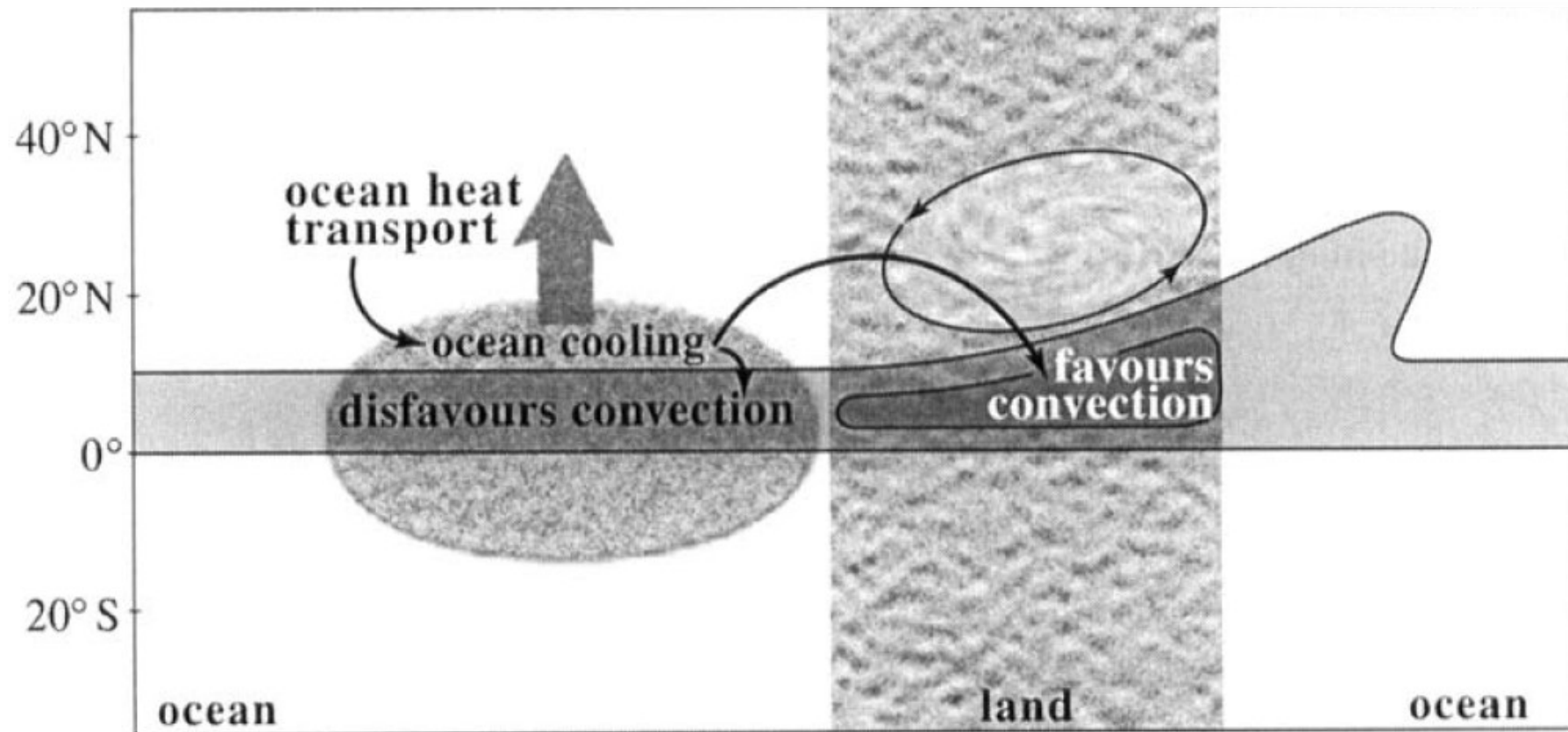
PROCESOS QUE AFECTAN LA CONVECCION SOBRE UN CONTINENTE IDEALIZADO EN VERANO



FEEDBACKS CON HUMEDAD DEL SUELO: (-) HS → (-) ET → (-) P → (-) HS

Ch&N (2001) comparan simulaciones con HS saturada (prescripta) versus simulaciones con HS interactuando con la atmósfera

PROCESOS QUE AFECTAN LA CONVECCIÓN SOBRE UN CONTINENTE IDEALIZADO EN VERANO

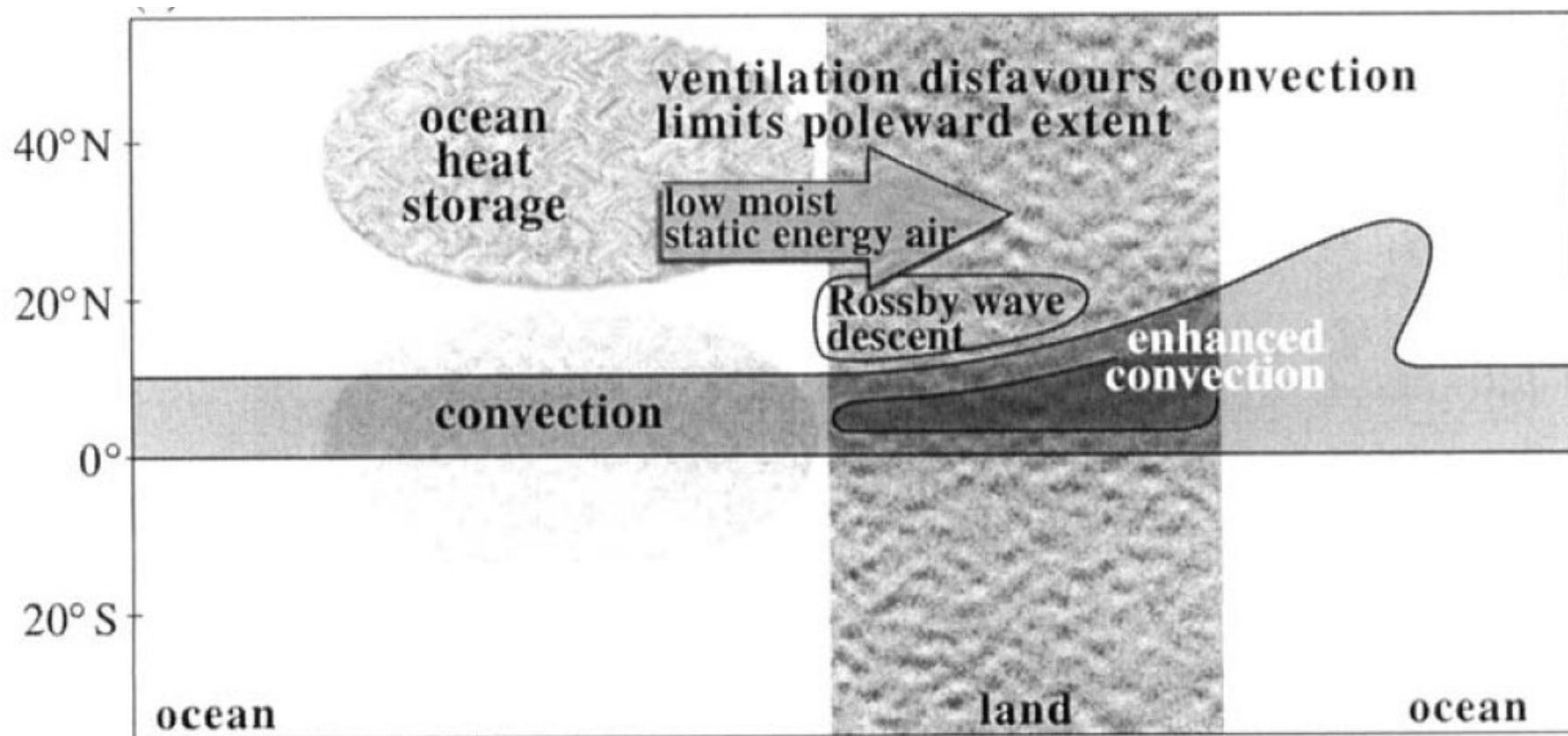


TRANSPORTE MERIDIONAL DE CALOR POR LOS OCEANOS: disminuye la SST en los trópicos y el gradiente de SST entre el ecuador y latitudes medias. En comparación, el continente en latitudes tropicales se torna una fuente de calor (en términos de flujo neto de calor hacia la atmósfera)

Ch&N (2001) comparan simulaciones con y sin transporte de calor a través del océano

Chou & Neelin (QJRMS, 2001)

PROCESOS QUE AFECTAN LA CONVECCIÓN SOBRE UN CONTINENTE IDEALIZADO EN VERANO



VENTILACION POR FLUJO CROS-CONTINENTAL: en los subtrópicos la advección de aire frío inhibe la convección principalmente del lado oeste y limita la extensión meridional del monzón. **MECANISMO INTERACTIVO DE RODWELL-HOSKINS:** en los trópicos la convección interactúa con los patrones de divergencia/convergencia de una onda de Rossby → contribuye a la asimetría zonal de la convección sobre el continente

Ch&N (2001) comparan simulaciones “prendiendo/apagando” estos mecanismos

CAMBIO CLIMATICO

Global Overview & changes

Monsoons strength and timing is related to atmospheric moisture content, land–sea temperature contrast, land cover and use, atmospheric aerosol loadings and other factors.

Global land monsoon precipitation: decreasing trend over the last half-century, with primary contributions from the weakened summer monsoon systems in the NH (Wang and Ding, 2006).

Combined global ocean–land monsoon precipitation has intensified during 1979–2008, mainly due to an upward trend in the NH summer oceanic monsoon precipitation (Zhou et al., 2008b; Hsu et al., 2011; Wang et al., 2012b).

Global Overview & changes (cont.)

Because the fractional increase in monsoon area is greater than that in total precipitation, the ratio of the latter to the former (a measure of the global monsoon intensity) exhibits a decreasing trend (Hsu et al., 2011).

CMIP5 models generally reproduce the observed global monsoon domain, but the disparity between the best and poorest models is large.

Algunas definiciones...

- *Global monsoon area (GMA): where the annual range of precipitation exceeds 2.5 mm day⁻¹. Here, the annual range is defined as the difference between the May to September (MJJAS) mean and the November to March (NDJFM) mean.
- *Global monsoon total precipitation (GMP): the mean of summer rainfall in the monsoon area.
- *Global monsoon precipitation intensity (GMI) : GMP divided by GMA.
- *In the CMIP5 models the global monsoon area (GMA), the global monsoon total precipitation (GMP) and the global monsoon precipitation intensity (GMI) are projected to increase by the end of the 21st century (2081–2100, Figure 14.1).
- *Daily precipitation intensity index (SDII): total precipitation divided by the number of days with precipitation greater than or equal to 1 mm

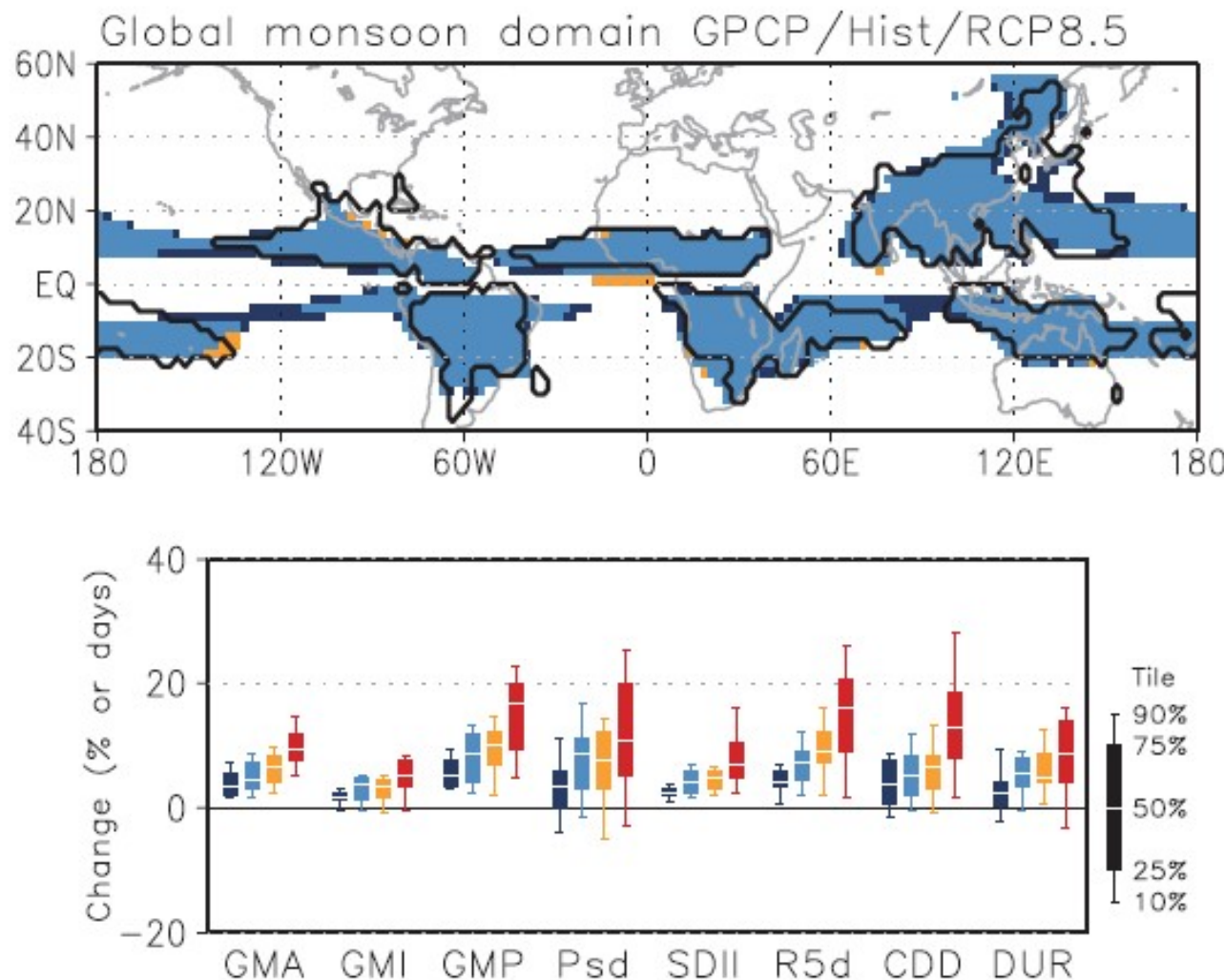


Figure 14.1 | (Upper) Observed (thick contour) and simulated (shading) global monsoon domain, based on the definition of Wang et al. (2011). The observations are based on GPCP v2.2 data (Huffman et al., 2009), and the simulations are based on 26 CMIP5 multi-model mean precipitation with a common 2.5 by 2.5 degree grid in the present day (1986–2005) and the future (2080–2099; RCP8.5 scenario). Orange (dark blue) shading shows monsoon domain only in the present day (future). Light blue shading shows monsoon domain in both periods. (Lower) Projected changes for the future (2080–2099) relative to the present day (1986–2005) in the global monsoon area (GMA) and global monsoon intensity (GMI), global monsoon total precipitation (GMP), standard deviation of interannual variability in seasonal average precipitation (Psd), simple daily precipitation intensity index (SDII), seasonal maximum 5-day precipitation total (R5d), seasonal maximum consecutive dry days (CDD) and monsoon season duration (DUR), under the RCP2.6 (dark blue; 18 models), RCP4.5 (light blue; 24 models), RCP6.0 (orange; 14 models) and RCP8.5 scenarios (red; 26 models). Units are % except for DUR (days). Box-and-whisker plots show the 10th, 25th, 50th, 75th and 90th percentiles. All of the indices are calculated for the summer season (May to September in the Northern Hemisphere; November to March in the Southern Hemisphere). The indices of Psd, SDII, R5d and CDD calculated for each model's original grid, and then averaged over the monsoon domains determined by each model at the present-day. The indices of DUR are calculated for seven regional monsoon domains based on the criteria proposed by Wang and LinHo (2002) using regionally averaged climatological cycles of precipitation, and then their changes are averaged with weighting based on their area at the present day.

Time series of anomalies over the global land monsoon domain relative to the present-day (1986–2005), based on CMIP5 multi-model monthly outputs

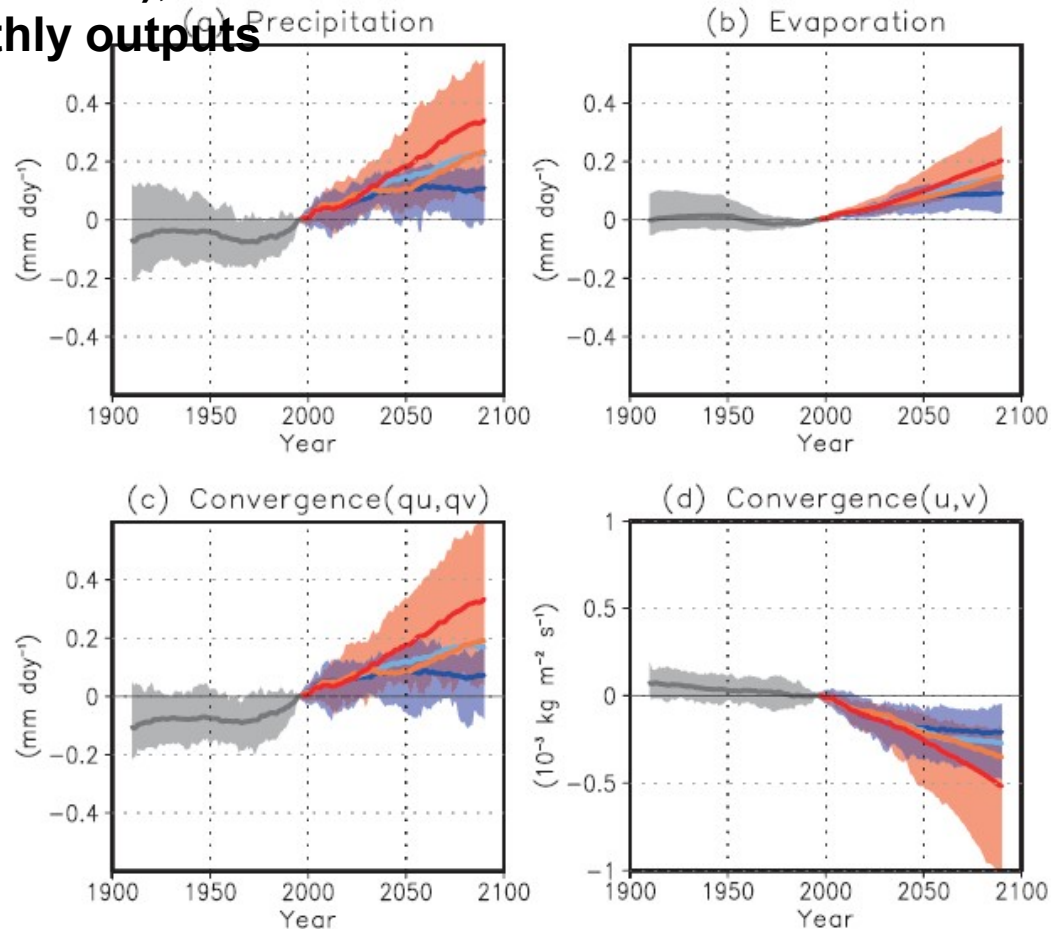


Figure 14.2 | Time series of simulated anomalies, smoothed with a 20-year running mean over the global land monsoon domain for (a) precipitation (mm day^{-1}), (b) evaporation (mm day^{-1}), (c) water vapour flux convergence in the lower (below 500 hPa) troposphere (mm day^{-1}), and (d) wind convergence in the lower troposphere ($10^{-3} \text{ kg m}^{-2} \text{ s}^{-1}$), relative to the present-day (1986–2005), based on CMIP5 multi-model monthly outputs. Historical (grey; 29 models), RCP2.6 (dark blue; 20 models), RCP4.5 (light blue; 24 models), RCP6.0 (orange; 16 models), and RCP8.5 (red; 24 models) simulations are shown in the 10th and 90th percentile (shading), and in all model averages (thick lines).

... however the localized effects of climate change on regional monsoon strength and variability are complex and more uncertain.

CMIP5 models show:

- a decreasing trend of lower-troposphere wind convergence (dynamical factor) throughout the 20th and 21st centuries (Fig.d).
- With increased moisture, the moisture flux convergence shows an increasing trend from 1980 through the 21st century (Fig.c).
- Surface evaporation shows a similar trend (Fig.b) associated with warmer SSTs.
- Therefore, the global monsoon precipitation increases (Fig.a) due to increases in moisture flux convergence and surface evaporation despite a weakened monsoon circulation.

The aerosol direct forcing may heat the atmosphere but cools the surface, altering atmospheric stability and inducing horizontal pressure gradients that modulate the large-scale circulation and hence monsoon rainfall (Lau et al., 2008). However, the representation of aerosol forcing differs among models, and remains an important source of uncertainty, particularly in some regional monsoon systems.

TENDENCIA OBSERVADA EN LA PRECIPITACION DEL MONZON GLOBAL

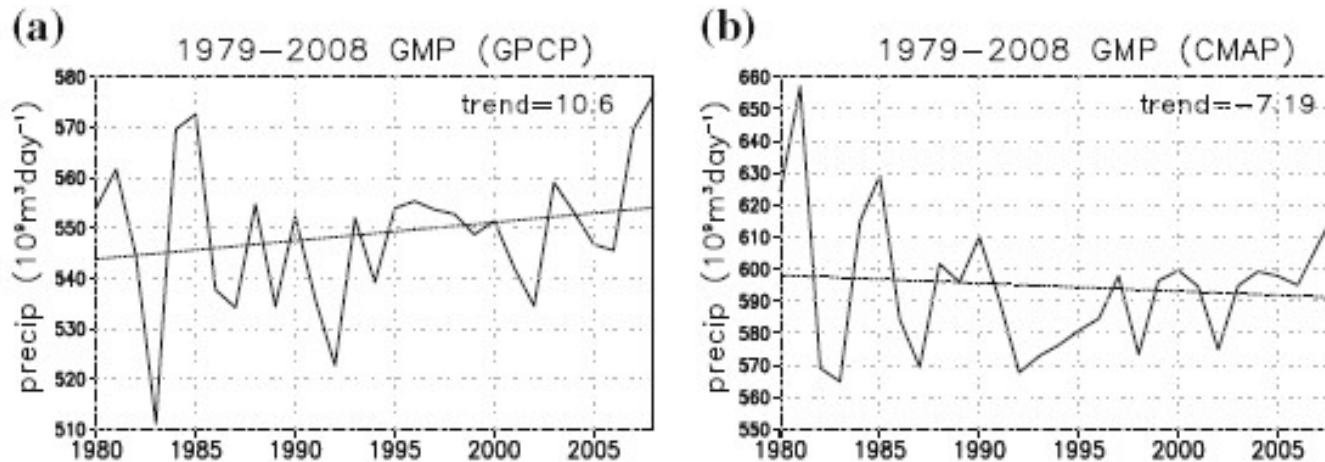
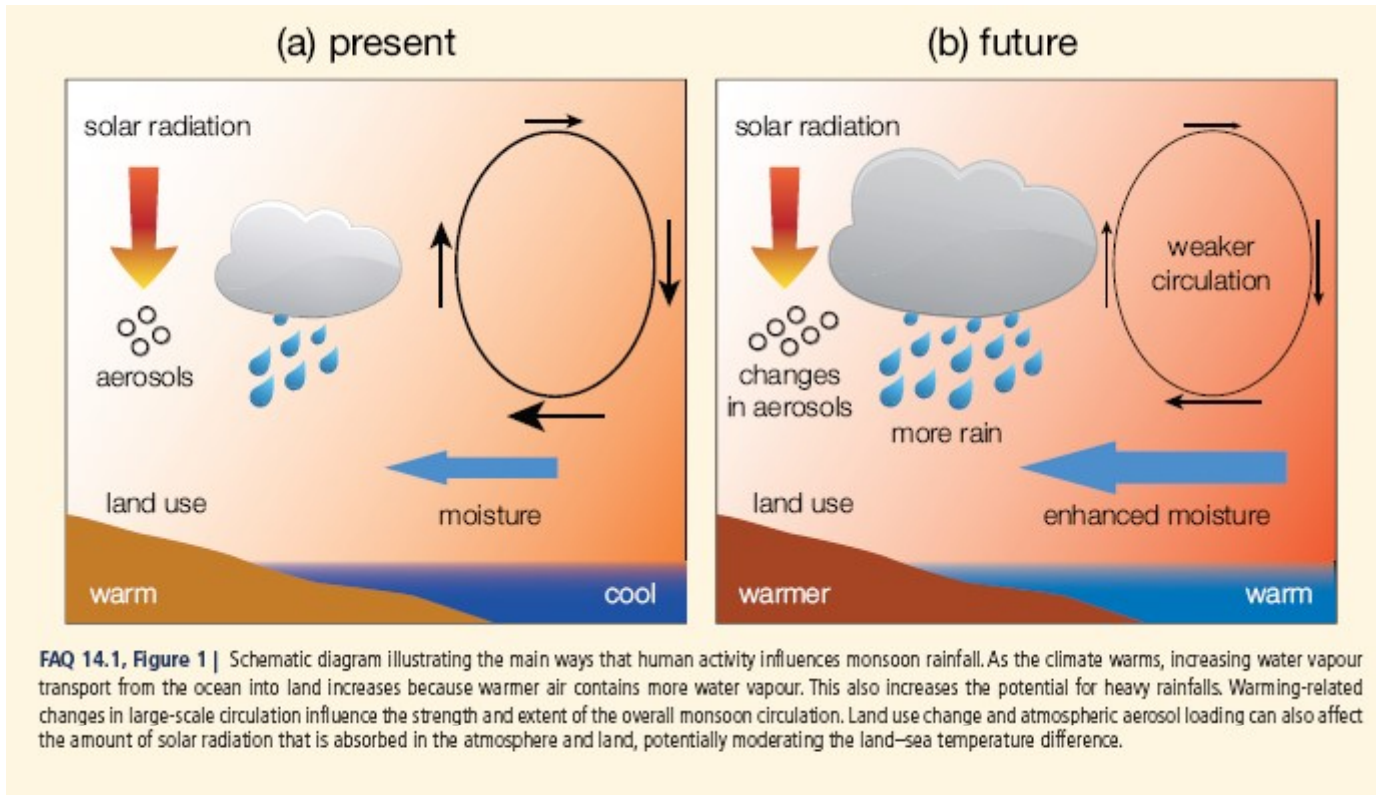


Fig. 2.3 **a** Time series of global monsoon precipitation (GMP; units: $10^9 \text{ m}^3 \text{ day}^{-1}$) calculated from (s) the GPCP and **b** the CMAP datasets for 1979–2008. The linear trend of each time series is indicated by a *dotted line*, with the linear trend [units: $10^9 \text{ m}^3 \text{ day}^{-1}(29 \text{ year})^{-1}$] noted on each panel. (Adapted from Hsu et al. 2011)

precipitation from the satellite data (Gruber et al. 2000).

The trends in global oceanic monsoon rainfall have dominated the trends in total GMP over the past three decades (Wang and Ding 2006; Zhou et al. 2008b; Hsu et al. 2011). The GMP showed an increasing trend from 1979 to 2008 based on the GPCP rainfall data, while it revealed a downward tendency over the same period using the CMAP dataset (Fig. 2.3). Zhou et al. (2008b) found that the oceanic monsoon rainfall derived from the GPCP dataset was highly correlated with that of the Special Sensor Microwave Imager (SSM/I), which might be the best available precipitation estimates over the ocean. This suggests that the trend in GMP obtained from the GPCP data is probably more reliable than that from the CMAP data. With a focus on the monsoon change at the hemispheric scale, Wang et al. (2013) found consistent enhancements of NH monsoon rainfall and of the Walker and Hadley circulations from 1979 to 2011.



FAQ 14.1, Figure 1 | Schematic diagram illustrating the main ways that human activity influences monsoon rainfall. As the climate warms, increasing water vapour transport from the ocean into land increases because warmer air contains more water vapour. This also increases the potential for heavy rainfalls. Warming-related changes in large-scale circulation influence the strength and extent of the overall monsoon circulation. Land use change and atmospheric aerosol loading can also affect the amount of solar radiation that is absorbed in the atmosphere and land, potentially moderating the land-sea temperature difference.

Strongest effect of climate change on the monsoons: the increase in atmospheric moisture associated with warming of the atmosphere, resulting in an increase in total monsoon rainfall even if the strength of the monsoon circulation weakens or does not change.

Future regional trends in monsoon intensity and timing remain uncertain in many parts of the world. Year-to-year variations in the monsoons in many tropical regions are affected by ENSO. How ENSO will change in future—and how its effects on monsoon will change—also remain uncertain.

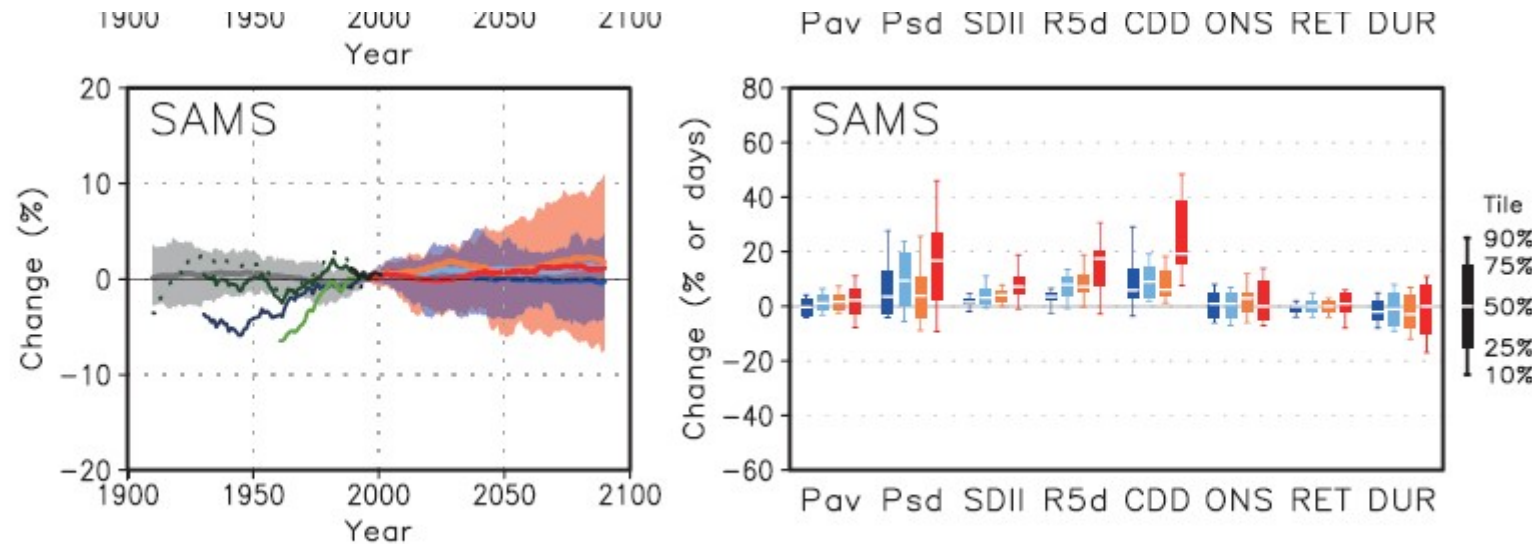


Figure 14.6 | As in Figure 14.4, except for (upper) North America Monsoon System (NAMS) and (lower) South America Monsoon System (SAMS).

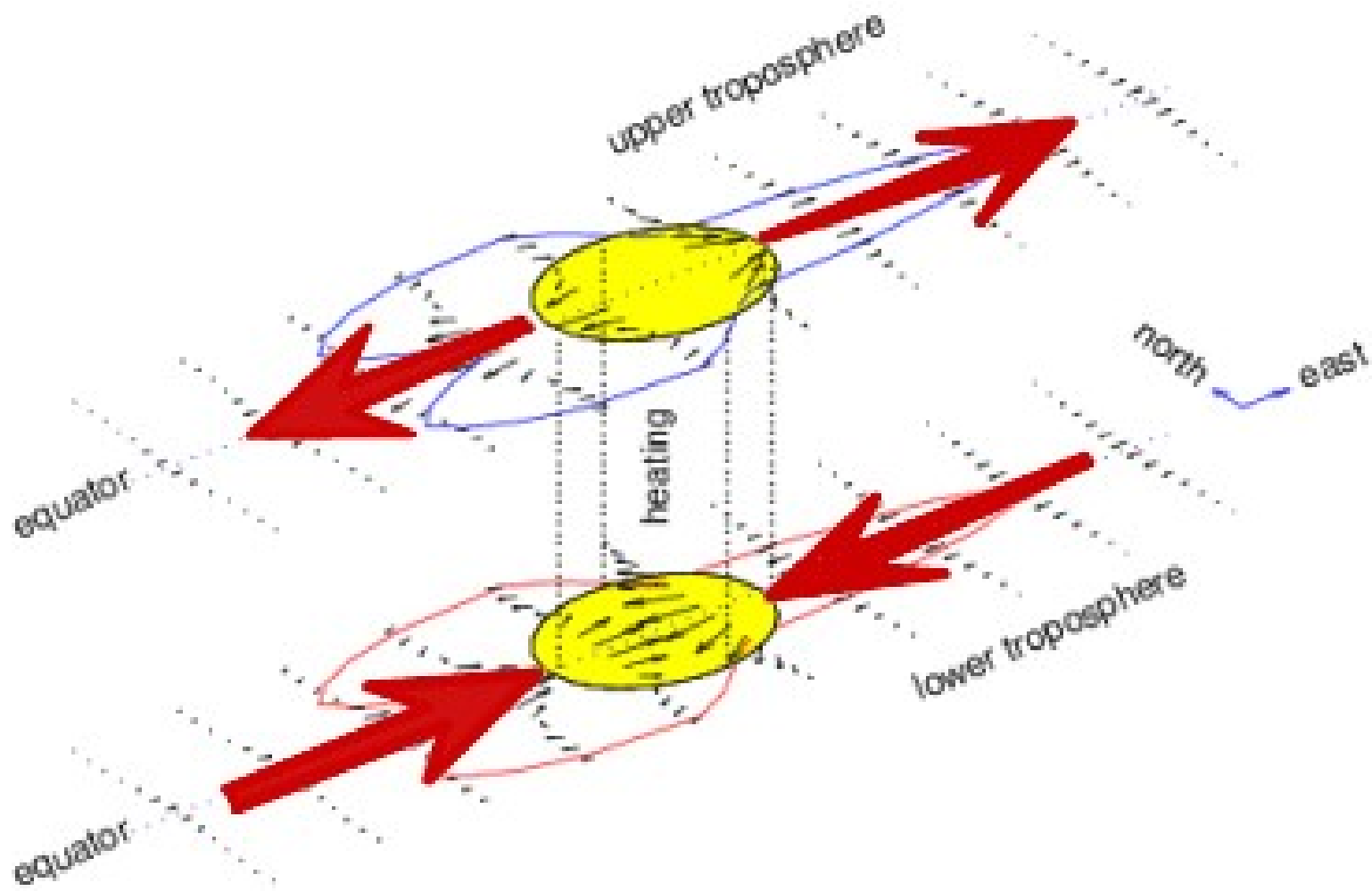
(Left) Time series of observed and model-simulated summer precipitation anomalies (%) relative to the present-day average.

There is medium confidence that SAMS overall precipitation will remain unchanged. The different estimates of changes in timing underscores potential uncertainties related to SAMS timing due to differences in SAMS indices. The models do show significant and robust increases in extreme precipitation indices in the SAMS region, such as seasonal maximum 5-day precipitation total and number of consecutive dry days (Figure 14.6), leading to medium confidence in projections of these characteristics.

APENDICE

a

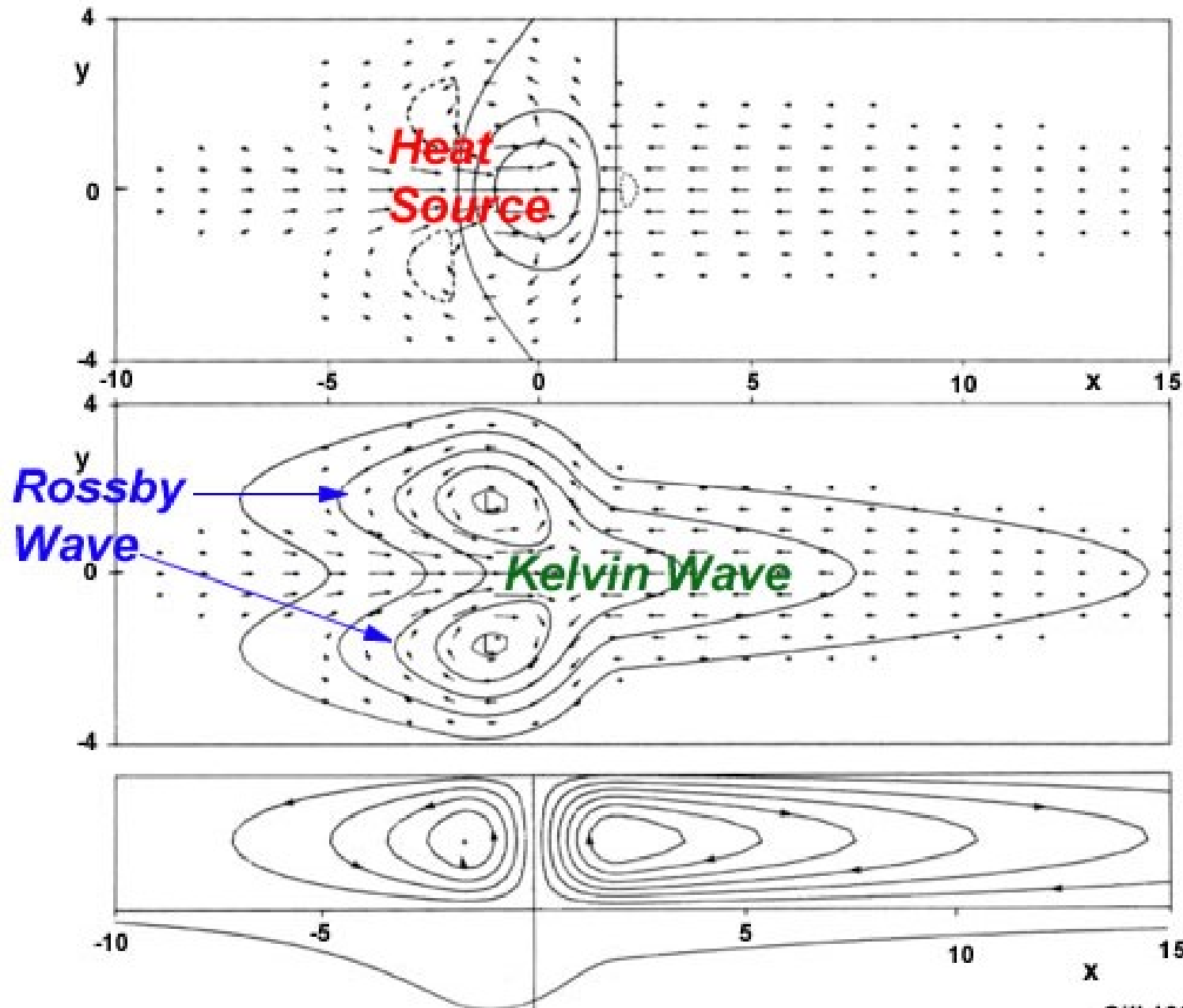
Two-Layer Model of Equatorial Heating



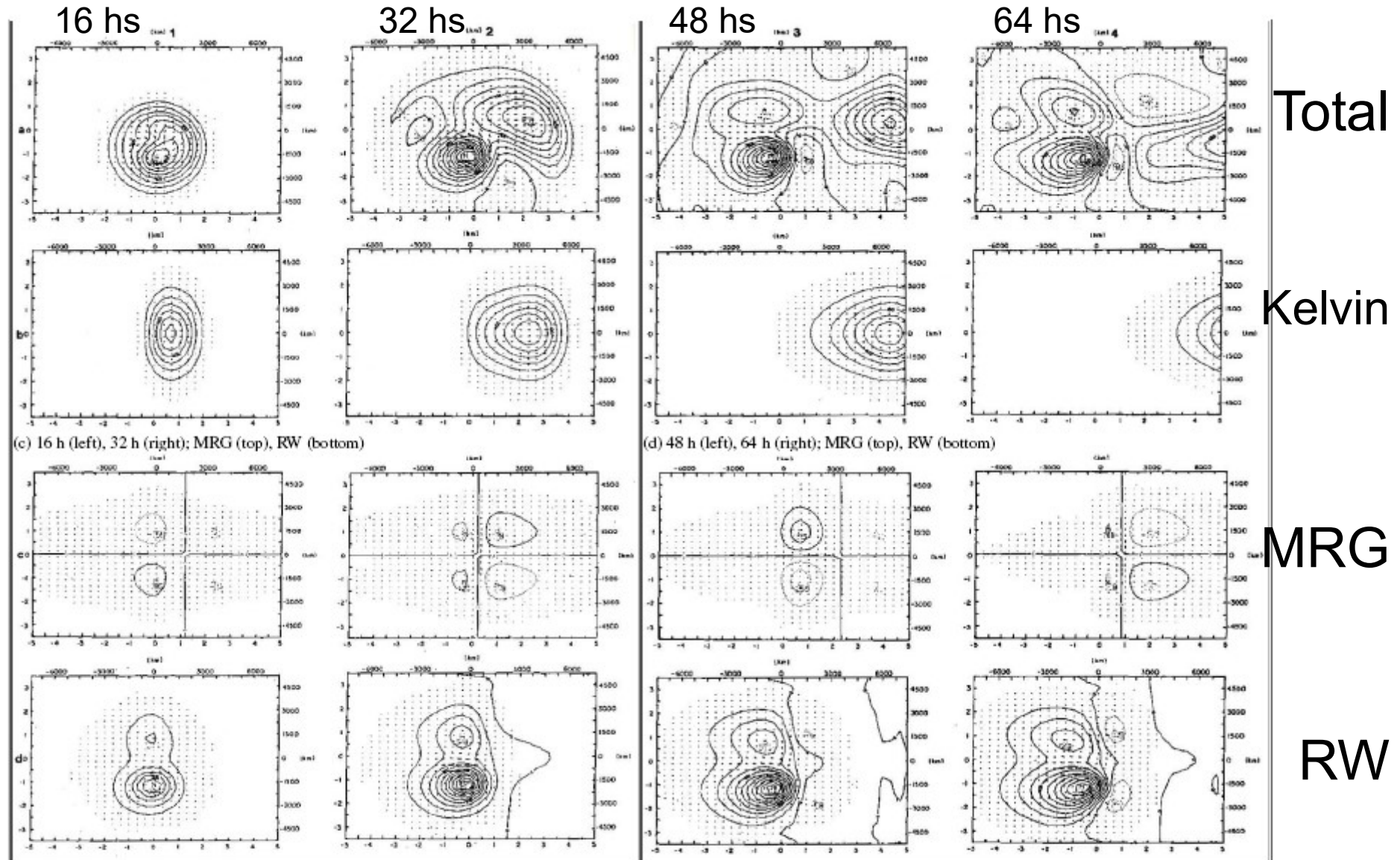
Gill, 1980

b

Equatorial Heating and Dynamical Response



Contribuciones de ondas de Kelvin, MRG y RW al campo total



Silva Dias et al 1983
Large-Scale Response of the Tropical Atmosphere to Transient Convection

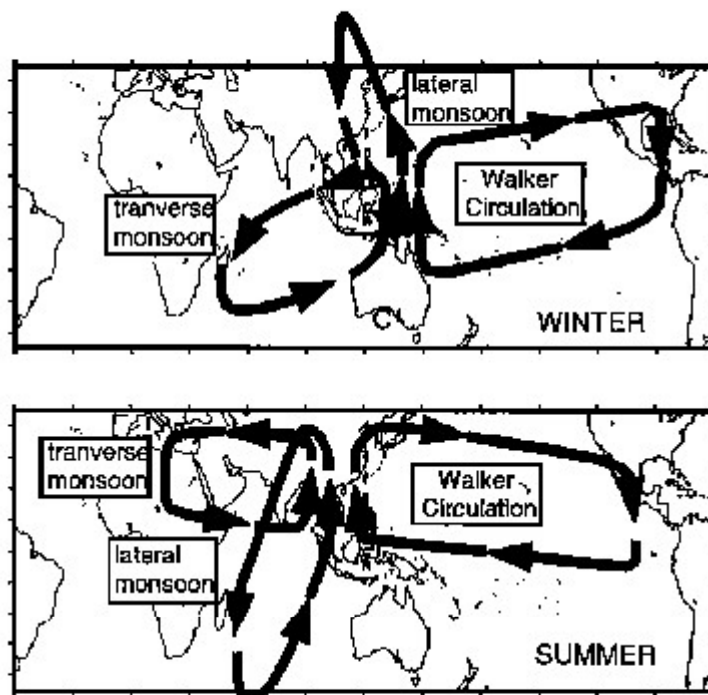
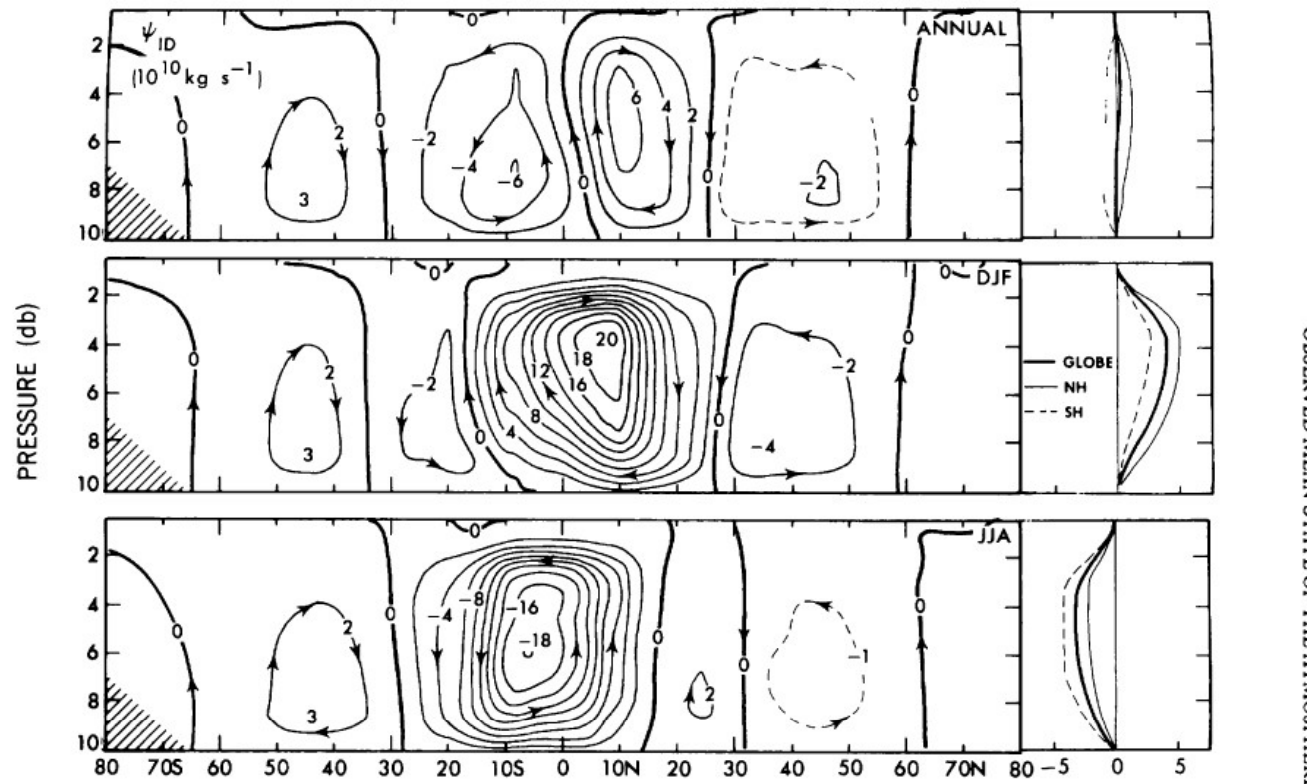


Figure 9. Synthesis of the summer and winter monsoon divergent wind circulations. Three major components are identified: the transverse monsoon, the lateral monsoon and the Walker Circulation. The lower tropospheric mass flux and the latent and radiative heating gradients associated with each circulation are given in Table 1 in units of Gkg and $\text{W m}^{-2} 1000 \text{ km}^{-1}$, respectively.



OBSERVED MEAN STATE OF THE ATMOSPHERE

FIGURE 7.19. Zonal-mean cross sections of the mass stream function in $10^{10} \text{ kg s}^{-1}$ for annual, DJF, and JJA mean conditions. Vertical profiles of the hemispheric and global mean values are shown on the right.

